r3_cmc: Three-Terminal Nonlinear (Diffused and Poly-Silicon) Resistor Model and JFET Model

Revision History

Release	Date	Authors	Comments
1.1.0	06/01/2020	G. J. Coram and C. C. McAndrew	
1.0.0	06/12/2007	C. C. McAndrew	Initial release.

Review History

Revision	Date	Reviewers

This work is licensed under the Creative Commons Attribution 4.0 International License. To view a copy of this license, visit http://creativecommons.org/licenses/by/4.0/ or send a letter to Creative Commons, PO Box 1866, Mountain View, CA 94042, USA.

Contents

1 Introduction **3**

2 Usage **3**

3 Instance Parameters **4**

4 Special Model Parameters **5**

5 Model Parameters **6**

6 Geometry Dependence **10**

7 Temperature Dependence **14**

8 Bias Dependence of Resistor Body Current **16**

9 Bias Dependence of Parasitics **18**

10 Noise **20**

11 Operating Point Information **21**

12 Statistical Variation **22**

13 Notes on Parameter Extraction **25**

14 References **30**

1 Introduction

The `r3_cmc` model is a nonlinear 3-terminal resistor model that includes self-heating, velocity saturation, statistical variations, and parasitic capacitances and currents. The core depletion pinching model formulation is for *p-n* junctions of diffused resistors, but it is also applicable for the MOS behavior of polysilicon resistors. As *p-n* junction depletion pinching controls JFET device behavior, the `r3_cmc` model is also applicable to JFETs.

NOTE: in this documentation parameters are set in `Courier` font, to distinguish them from other quantities.

2 Usage

(NOTE: exact usage may be simulator dependent; e.g. whether the local temperature rise port for self-heating is made available or not, and whether the initial instance key-letter "r" is required.)

```
r<instanceName> (<n1> <nc> <n2>) <modelName> <instanceParameters>
.model <modelName> r3_cmc <modelParameters>
```

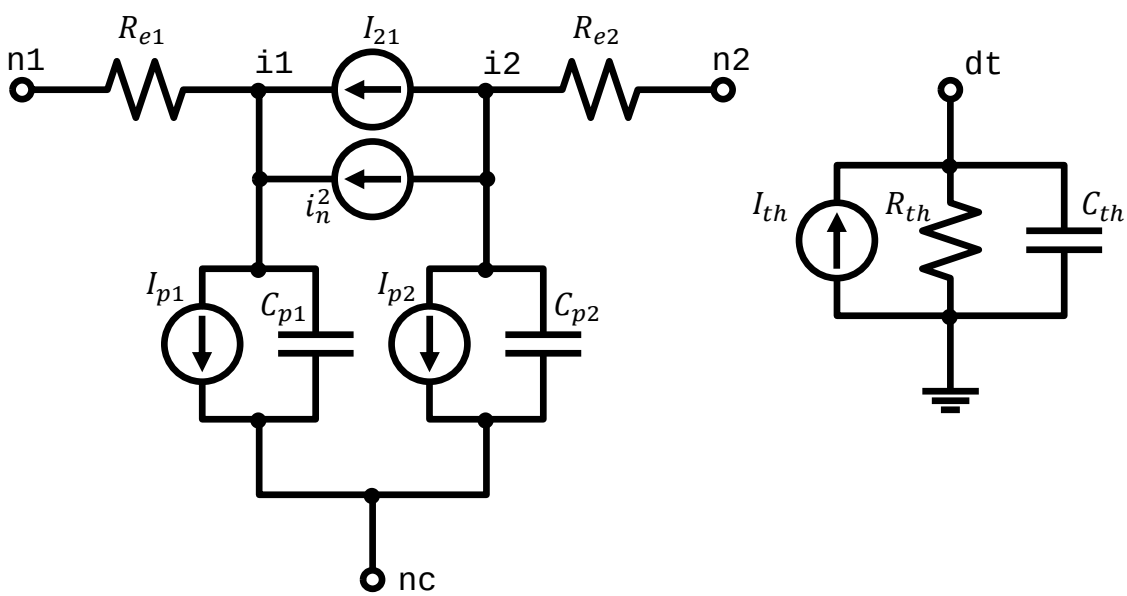

Figure 1: `r3_cmc` Model Equivalent Network.

3 Instance Parameters

Name	Default	Min.	Max.	Units	Description
w	10^{-6}	0.0	∞	m	design width of resistor body
l	10^{-6}	0.0	∞	m	design length of resistor body
wd	0.0	0.0	∞	m	dogbone width (total; not per side)
a1	0.0	0.0	∞	m^2	area of port n1 partition
p1	0.0	0.0	∞	m	perimeter of port n1 partition
c1	0	0	∞		number of contacts at n1 port
a2	0.0	0.0	∞	m^2	area of port n2 partition
p2	0.0	0.0	∞	m	perimeter of port n2 partition
c2	0	0	∞		number of contacts at n2 port
trise (dtemp)	0.0			^{o}C	local temperature offset from ambient (before self-heating)
sw_noise	1	0	1		switch for including noise: 0=no and 1=yes
sw_et	1	0	1		switch for self-heating: 0=exclude 1=include
sw_lin	0	0	1		switch to force linearity: 0=no and 1=yes
sw_mman	0	0	1		switch for mismatch analysis: 0=no and 1=yes
nsmm_rsh	0.0				number of σ's of local variation for rsh
nsmm_w	0.0				number of σ's of local variation for w
nsmm_l	0.0				number of σ's of local variation for l

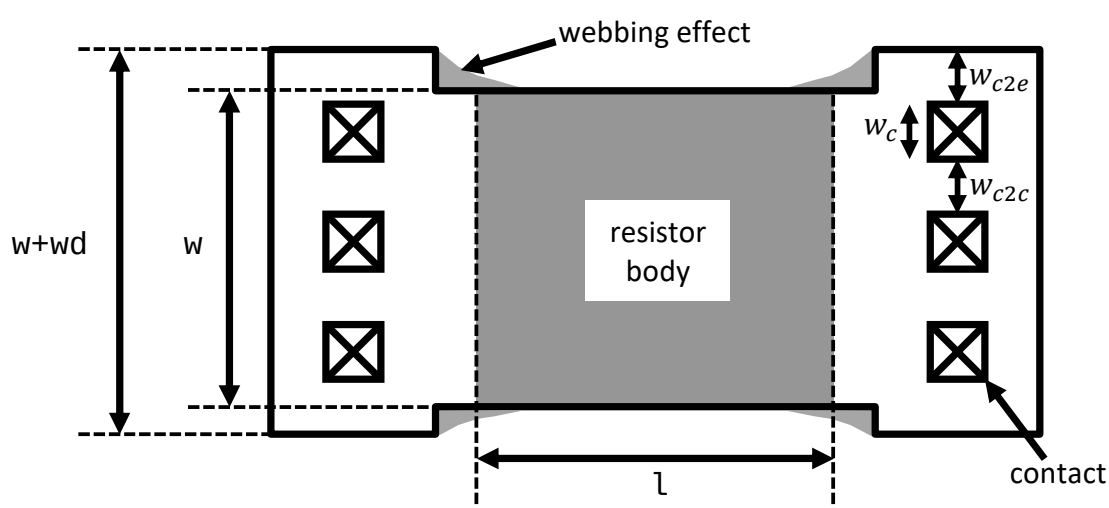

$\texttt{a[12]} = area(end[12]) + \texttt{w} \cdot \texttt{l}/2$

$\texttt{p[12]} = perim(end[12]) + \texttt{l}$ $\qquad \texttt{wd} = \texttt{c1} \cdot w_c + (\texttt{c1} - 1) \cdot w_{c2c} + 2w_{c2e} - \texttt{w}$

Figure 2: Instance Parameter examples, note that the end region dogbone may be asymmetric.

4 Special Model Parameters

Name	Default	Min.	Max.	Units	Description
`version`					model version (major model change)
`subversion`					model subversion (minor model change)
`revision`					model revision (implementation update)
`level`	1003				model level
`type`	-1	-1	+1		resistor type: -1=n-body and +1=p-body
`scale`	1.0	0.0	1.0		scale factor for instance geometries
`shrink`	0.0	0.0	100.0	%	shrink percentage for instance geometries
`tmin`	-100.0	-250.0	27.0	ºC	minimum ambient temperature
`tmax`	500.0	27.0	1000.0	ºC	maximum ambient temperature
`rthresh`	0.001	0.0	∞	Ω	threshold to switch end resistance to V=I*R form
`imax`	1.0	0.0	∞		current at which to linearize diode currents
`tnom`	27.0	-250.0	1000.0	ºC	nominal (reference) temperature
`lmin`	0.0	0.0	∞	μm	minimum allowed drawn length
`lmax`	9.9×10^9	`lmin`	∞	μm	maximum allowed drawn length
`wmin`	0.0	0.0	∞	μm	minimum allowed drawn width
`wmax`	9.9×10^9	`wmin`	∞	μm	maximum allowed drawn width
`jmax`	100.0	0.0	∞	A/μm	maximum current density
`vmax`	9.9×10^9	0.0	∞	V	maximum voltage w.r.t. control port `nc`
`tminclip`	-100.0	-250.0	27.0	ºC	clip minimum temperature
`tmaxclip`	500.0	27.0	1000.0	ºC	clip maximum temperature

5 Model Parameters

Name	Default	Min.	Max.	Units	Description
rsh	100.0	0.0	∞	$\Omega/\square$	sheet resistance
xw	0.0			μm	width offset (total)
nwxw	0.0			μm2	narrow width width offset correction coefficient
wexw	0.0			μm	webbing effect width offset correction coefficient (for dog-boned devices)
fdrw	1.0	0.0	∞	μm	finite doping width offset reference width
fdxwinf	0.0			μm	finite doping width offset width value for wide devices
xl	0.0			μm	length offset (total)
xlw	0.0				width dependence of length offset
dxlsat	0.0			μm	additional length offset for velocity saturation calculation
nst	1.0	0.1	5.0		subthreshold slope parameter
ats (atsinf)	0.0				V saturation smoothing parameter
atsl	0.0			Vμm	saturation smoothing parameter 1/l coefficient
dfinf	0.01	0.0001	10.0	$/\sqrt{\text{V}}$	depletion factor for wide/long device
dfl	0.0			μm $/\sqrt{\text{V}}$	depletion factor 1/l coefficient
dfw	0.0			μm $/\sqrt{\text{V}}$	depletion factor 1/w coefficient
dfwl	0.0			μm$^2/\sqrt{\text{V}}$	depletion factor 1/(w*l) coefficient
sw_dfgeo	1	0	1		switch for depletion factor geometry dependence: 0=drawn and 1=effective
dp (dpinf)	2.0	0.1	∞	V	depletion potential
dpl	0.0			(Vμm)^{dple}	depletion potential l dependence coefficient
dple	1.0				depletion potential l dependence exponent
dpw	0.0			(Vμm)^{dpwe}	depletion potential w dependence coefficient
dpwe	1.0				depletion potential w dependence exponent

Name	Default	Min.	Max.	Units	Description
dpwl	0.0			$(\mathrm{V}\mu\mathrm{m})^{\mathrm{dpwe+dple}}$	depletion potential wl dependence coefficient
ecrit	4.0	0.02	1000.0	V/μm	velocity saturation critical field
ecorn	0.4	0.01	ecrit	V/μm	velocity saturation corner field
sw_vsatt	0	0	1		switch for vsat temperature effects: 0=none and 1=link with body resistance
sw_accpo	0	0	3		switch for pinch-off modeling
grpo	10^{-12}	0	0.1		minimum body conductance in pinch-off
du	0.02	0.0	1000.0		mobility reduction at ecorn
rc	0.0	0.0	∞	Ω	resistance per contact
rcw	0.0	0.0	∞	$\Omega\mu$m	width adjustment for contact resistance
fc	0.9	0.0	0.99		depletion capacitance linearization factor
isa	0.0	0.0	∞	A/μm^2	diode saturation current per unit area
na	1.0	0.0	∞		ideality factor for isa
ca	0.0	0.0	∞	F/μm^2	fixed capacitance per unit area
cja	0.0	0.0	∞	F/μm^2	depletion capacitance per unit area
pa	0.75	0.0	∞	V	built-in potential for cja
ma	0.33	0.0	1.0		grading coefficient for cja
aja	-0.5			V	smoothing parameter for cja
isp	0.0	0.0	∞	A/μm	diode saturation current per unit perimeter
np	1.0	0.0	∞		ideality factor for isp
cp	0.0	0.0	∞	F/μm	fixed capacitance per unit perimeter
cjp	0.0	0.0	∞	F/μm	depletion capacitance per unit perimeter
pp	0.75	0.0	∞	V	built-in potential for cjp
mp	0.33	0.0	1.0		grading coefficient for cjp
ajp	-0.5			V	smoothing parameter for cjp
vbv	0.0	0.0	∞	V	breakdown voltage
ibv	10^{-6}	0.0	∞	A	current at breakdown
nbv	1.0	0.0	∞		ideality factor for breakdown current

Name	Default	Min.	Max.	Units	Description
kfn	0.0	0.0	∞		flicker noise coefficient (unit depends on afn)
afn	2.0	0.0	∞		flicker noise current exponent
bfn	1.0	0.0	∞		flicker noise 1/f exponent
sw_fngeo	0	0	1		switch for flicker noise geometry calculation: 0=drawn 1=effective
ea	1.12			V	activation voltage for diode temperature dependence
xis	3.0				exponent for diode temperature dependence
tc1	0.0			/K	resistance linear TC
tc2	0.0			/K^2	resistance quadratic TC
tc1l	0.0			μm/K	resistance linear TC 1/l coefficient
tc2l	0.0			μm/K^2	resistance quadratic TC 1/l coefficient
tc1w	0.0			μm/K	resistance linear TC 1/w coefficient
tc2w	0.0			μm/K^2	resistance quadratic TC 1/w coefficient
tc1wl	0.0			μm^2 /K	resistance linear TC 1/(wl) coefficient
tc2wl	0.0			μm^2 /K^2	resistance quadratic TC 1/(wl) coefficient
tc1rc	0.0			/K	contact resistance linear TC
tc2rc	0.0			/K^2	contact resistance quadratic TC
tc1dp	0.0			/K	depletion potential linear TC
tc2dp	0.0			/K^2	depletion potential quadratic TC
tc1kfn	0.0			/K	flicker noise coefficient linear TC
tc1vbv	0.0			/K	breakdown voltage linear TC
tc2vbv	0.0			/K^2	breakdown voltage quadratic TC
tc1nbv	0.0			/K	breakdown ideality factor linear TC
tegth	0.0	-∞	0.0		thermal conductance temperature exponent
gth0	10^6	0.0	∞	W/K	thermal conductance fixed component
gthp	0.0	0.0	∞	W/Kμm	thermal conductance perimeter component
gtha	0.0	0.0	∞	W/Kμm^2	thermal conductance area component
gthc	0.0	0.0	∞	W/K	thermal conductance contact component
cth0	0.0	0.0	∞	sW/K	thermal capacitance fixed component
cthp	0.0	0.0	∞	sW/Kμm	thermal capacitance perimeter component
ctha	0.0	0.0	∞	sW/Kμm^2	thermal capacitance area component
cthc	0.0	0.0	∞	sW/K	thermal capacitance contact component

Name	Default	Min.	Max.	Units	Description
nsig_rsh	0.0				number of standard deviations of global variation for rsh
nsig_w	0.0				number of standard deviations of global variation for w
nsig_l	0.0				number of standard deviations of global variation for l
sig_rsh	0.0	0.0	∞	%	global variation standard deviation for rsh (relative)
sig_w	0.0	0.0	∞	μm	global variation standard deviation for w (absolute)
sig_l	0.0	0.0	∞	μm	global variation standard deviation for l (absolute)
smm_rsh	0.0	0.0	∞	% μm	local variation standard deviation for rsh (relative)
smm_w	0.0	0.0	∞	$\mu m^{1.5}$	local variation standard deviation for w (absolute)
smm_l	0.0	0.0	∞	$\mu m^{1.5}$	local variation standard deviation for l (absolute)
sw_mmgeo	0	0	1		switch for flicker noise geometry calculation: 0=drawn and 1=effective

6 Geometry Dependence

Unless otherwise noted, all r3_cmc model quantities scale with the multiplicity factor $mfactor as defined in the Verilog-A Language Reference Manual (LRM), version 2.4 [1].

The r3_cmc model includes several mechanisms for deviations of the effective electrical length and width of a resistor from the drawn (design, or mask) values. The drawn length and width of the resistor, in units of microns, are

$$l_um = \mathtt{l} \cdot \mathtt{scale} \cdot (1 - \mathtt{shrink}/100) \cdot 10^6, \tag{1}$$

$$w_um = \mathtt{w} \cdot \mathtt{scale} \cdot (1 - \mathtt{shrink}/100) \cdot 10^6. \tag{2}$$

Because subcircuit models for resistors can consist of multiple resistance sections connected in series, it is desirable to be able to switch on and off the "end corrections" for length to facilitate implementation of such multi-section models. This is the function of the c1 and c2 instance parameters of the r3_cmc model. The effective length offset is

$$xleff = (\mathtt{xl} + \mathtt{xlw}/w_um) \cdot \big((\mathtt{c1} > 0) + (\mathtt{c2} > 0)\big)/2 \tag{3}$$

(which is zero if neither end is contacted, $\mathtt{xl} + \mathtt{xlw}/w_um$ if both ends are contacted, and one half of the latter if only one end is contacted). The effective electrical length, in microns, is

$$leff_um = l_um + xleff. \tag{4}$$

For flexibility of separately fitting low bias resistance and velocity saturation, an additional offset dxlsat is added to for calculation of the electric field used in the velocity saturation model (2).

The effective width offset includes the physical effect models derived in [2]. These comprise a fixed offset for mask bias, lithography, and etching effects, and geometry dependent offsets for LOCOS, the webbing effect, and the finite dopant source effect. The effective electrical width, in microns, is

$$weff_um = \frac{w_um + \mathtt{xw} + (\mathtt{nwxw}/w_um) + \mathtt{fdxinf} \cdot (1 - \exp(-w_um/\mathtt{fdrw}))}{1 - \mathtt{wexw} \cdot wd_um/(l_um \cdot w_um)} \tag{5}$$

where the width of the dogbone (see Fig. 2), for the webbing effect model, in units of microns, is

$$wd_um = \mathtt{wd} \cdot \mathtt{scale} \cdot (1 - \mathtt{shrink}/100) \cdot 10^6, \tag{6}$$

The depletion factor depends on geometry as

$$df = \mathtt{dfinf} + \frac{\mathtt{dfw}}{W} + \frac{\mathtt{dfl}}{L} + \frac{\mathtt{dfwl}}{WL} \tag{7}$$

where the width W and length L are effective geometries if $\mathtt{sw_geo} = 1$ and design geometries otherwise (in units of micron).

The depletion potential depends on geometry in version 1.1.0 as

$$dp_i = \mathtt{dp} \cdot \left(1 + \frac{\mathtt{dpw}}{W^{\mathtt{dpwe}}}\right) \cdot \left(1 + \frac{\mathtt{dpl}}{L^{\mathtt{dple}}}\right) \cdot \left(1 + \frac{\mathtt{dpwl}}{W^{\mathtt{dpwe}} L^{\mathtt{dple}}}\right). \tag{8}$$

(In version 1.0.0, $dp_i = \mathtt{dp}$.)

The zero-bias resistance, which factors in the zero-bias depletion pinching, is then

$$R_0 = \mathtt{rsh} \cdot \frac{\mathit{leff_um}}{\mathit{weff_um}} \cdot \left(1.0 - df\sqrt{dp_i}\right), \quad gf = 1/R_0. \tag{9}$$

Although end effects, such as spreading resistance and contact resistance, are assumed to be modeled via the `xl` parameter, the temperature coefficients of the end effects may differ from those of the body of the resistor. Simple analysis shows that these different temperature coefficients can be accounted for by introducing inverse length dependence to the temperature coefficients. A width dependence of temperature coefficients of resistance is also included in the model, and version 1.1.0 also includes an area dependence. Therefore, in `r3_cmc`

$$T_{C1}^{eff} = \mathtt{tc1} + \frac{\mathtt{tc1w}}{\mathit{weff_um}} + \frac{0.5 \cdot [(c1 > 0) + (c2 > 0)]}{\mathit{leff_um}} \cdot \left(\mathtt{tc1l} + \frac{\mathtt{tc1wl}}{\mathit{weff_um}}\right), \tag{10}$$

$$T_{C2}^{eff} = \mathtt{tc2} + \frac{\mathtt{tc2w}}{\mathit{weff_um}} + \frac{0.5 \cdot [(c1 > 0) + (c2 > 0)]}{\mathit{leff_um}} \cdot \left(\mathtt{tc2l} + \frac{\mathtt{tc2wl}}{\mathit{weff_um}}\right) \tag{11}$$

where the length dependence is switched on, off, or halved, depending on whether the resistor is contacted at both ends, not contacted, or contacted at only one end, respectively. The dependence of the temperature coefficients on whether a resistor is contacted or not enables consistent modeling of temperature coefficients for single or multiple section models.

The thermal conductance and capacitance include area, perimeter, contact, and fixed components. Asymptotically for a large area device, the heat flow is perpendicular to the plane of heat generation in the resistor, and the heat energy stored in a device depends on its volume, hence the area dependent component. For a long resistor, as it becomes narrower more of the heat flow is conducted by a "fringe" path at the edges of the device, hence the perimeter dependent component. As both length and width decrease, the thermal conditions in the device asymptotically approach that of a point source in an infinite medium, hence the fixed component. Contacts conduct heat flow, hence the contact component. The thermal conductance and capacitance are therefore

$$g_{TH} = \mathtt{gth0} + \mathtt{gthp} \cdot \mathit{p_um} + \mathtt{gtha} \cdot \mathit{a_um2} + \mathtt{gthc} \cdot (\mathtt{c1} + \mathtt{c2}) \tag{12}$$

$$c_{TH} = \mathtt{cth0} + \mathtt{cthp} \cdot \mathit{p_um} + \mathtt{ctha} \cdot \mathit{a_um2} + \mathtt{cthc} \cdot (\mathtt{c1} + \mathtt{c2}) \tag{13}$$

where the area and perimeter are calculated as

$$\mathit{a_um2} = \mathit{l_um} \cdot \mathit{w_um} \tag{14}$$

$$\mathit{p_um} = 2 \cdot \mathit{l_um} + [(\mathtt{c1} > 0) + (\mathtt{c2} > 0)] \cdot \mathit{w_um}. \tag{15}$$

The calculated perimeter therefore depends on whether the ends are contacted or not. Note that often the design dimensions of the body of a resistor differ from the overall dimensions of the device, for example if the design length is considered to be the unsalicided length of a poly resistor,

the total resistor length will typically include silicided contact regions. So it is not readily apparent what dimension should be used in calculation of the thermal conductance and capacitance. That is why the design dimensions, rather than some effective dimensions (whose value is calculated to best fit DC electrical data), are used. This turns out to be reasonable (with the exception that differences between the perimeter components along length and width dimensions are ignored), because if there is some difference Δ between design and effective dimensions for thermal conductance modeling, then for a device contacted at both ends

$$\begin{aligned} g_{TH} &= \mathtt{gth0} + \mathtt{gthp} \cdot (2 \cdot \mathit{l_um} + 2 \cdot \mathit{w_um} + 4 \cdot \Delta) + \mathtt{gtha} \cdot (\mathit{l_um} + \Delta)(\mathit{w_um} + \Delta) \\ &= \left(\mathtt{gth0} + 4 \cdot \mathtt{gthp} \cdot \Delta + \mathtt{gtha} \cdot \Delta^2\right) + (\mathtt{gthp} + 0.5 \cdot \mathtt{gtha} \cdot \Delta)\, \mathit{p_um} \\ &\quad + \mathtt{gtha} \cdot \mathit{a_um2} \end{aligned} \tag{16}$$

therefore any difference between design and effective dimensions can be taken into account by appropriate characterization of the fixed, perimeter, and area component parameters.

Because the "local" thermal conductance differs between the edge of a device and the center of a device, it is higher at the edge because of "fringing" conductance, the temperature of a resistor undergoing self-heating is not spatially uniform, but rather it is lower at the edges than in the middle. This is not taken into account in the `r3_cmc` model.

The end resistances are calculated from the resistance per contact and the number of contacts (parallel to the width dimension; adding contacts parallel to the length dimension, which can be done for reliability purposes, does not alter the resistance much – unless the contact adjacent to the resistor body fails),

$$R_{e1} = \frac{\mathtt{rc} + \mathtt{rcw}/\mathit{w_um}}{\mathtt{c1}}, \quad R_{e2} = \frac{\mathtt{rc} + \mathtt{rcw}/\mathit{w_um}}{\mathtt{c2}}. \tag{17}$$

The velocity saturation model includes geometry dependence in the bias dependent portion of the model evaluation, as it is formulated in terms of the electric field $E = V_{21}/(\mathit{leff_um} + \mathtt{dxlsat})$.

The areas and perimeters of the end region partitions, used in parasitic calculations, are, in units of microns,

$$\mathit{p1_um} = \mathtt{p1} \cdot \mathtt{scale} \cdot (1 - \mathtt{shrink}/100) \cdot 10^6, \tag{18}$$

$$\mathit{a1_um} = \mathtt{a1} \cdot \left[\mathtt{scale} \cdot (1 - \mathtt{shrink}/100) \cdot 10^6\right]^2, \tag{19}$$

$$\mathit{p2_um} = \mathtt{p2} \cdot \mathtt{scale} \cdot (1 - \mathtt{shrink}/100) \cdot 10^6, \tag{20}$$

and

$$\mathit{a2_um} = \mathtt{a2} \cdot \left[\mathtt{scale} \cdot (1 - \mathtt{shrink}/100) \cdot 10^6\right]^2. \tag{21}$$

If the number of contacts is not known, it can be calculated (see Fig. 2). Let the contact width (in the direction parallel to the resistor width) be w_c, the minimum spacing from a contact to the edge of the region it is in at the contact head of the resistor be w_{c2e}, and the (minimum) spacing between

contacts be w_{c2c}. If (as in some older technologies) contacts can be scaled, then `rc` should be set to be the resistance of a minimum width contact and

$$c[1,2] = \frac{\max(\mathtt{w} + \mathtt{wd}, w_c + 2 \cdot w_{c2e}) - 2 \cdot w_{c2e}}{w_c} \tag{22}$$

and for technologies where the contact width is fixed (assuming the maximum possible number of contacts are places)

$$c[1,2] = \text{int}\left[\frac{\max(\mathtt{w} + \mathtt{wd}, w_c + 2 \cdot w_{c2e}) - 2 \cdot w_{c2e} + w_{c2c}}{w_c + w_{c2c}}\right]. \tag{23}$$

7 Temperature Dependence

The zero-bias resistance R_0 varies with temperature as

$$R_0(T) = R_0 \cdot \mathit{tfac} \tag{24}$$

where R_0 is the nominal value of the zero-bias resistance (9) at the nominal temperature `tnom` and *tfac* is the resistor temperature factor, given by

$$\mathit{tfac} = \left(1 + T_{C1}^{eff} \cdot dT + T_{C2}^{eff} \cdot dT^2\right) \tag{25}$$

where dT is the temperature difference (including self-heating) with respect to `tnom`, and T_{C1}^{eff} and T_{C2}^{eff} are first (linear) and second (quadratic) order effective temperature coefficients, from (10) and (11), respectively. Smooth limiting of the resistance temperature factor *tfac* in (25) is implemented to a minimum value of 0.01. The conductance factor in (40) is then

$$gf = 1/R_0(T). \tag{26}$$

The depletion potential has a temperature dependence in version 1.1.0, given by

$$dp(T) = dp_i \cdot \left(1 + \mathtt{tc1dp} \cdot dT + \mathtt{tc2dp} \cdot dT^2\right). \tag{27}$$

The velocity saturation temperature dependence in version 1.1.0 is activated by the parameter `sw_vsatt`. If `sw_vsatt` $= 0$, then there is no temperature dependence; this is the default for compatibility reasons. If `sw_vsatt` $= 1$, then the corner and critical fields for velocity saturation are adjusted according to

$$ecorn(T) = \mathtt{ecorn} \cdot rT^{\mathtt{xvsat}} \cdot \mathit{tfac} \tag{28}$$

$$ecrit(T) = \mathtt{ecrit} \cdot rT^{\mathtt{xvsat}} \cdot \mathit{tfac} \tag{29}$$

where rT is the ratio of device to nominal temperature (in Kelvin), `xvsat` is a model parameter, and *tfac* is the same temperature factor as the resistor body.

The end resistances vary with temperature as

$$R_{e[1,2]}(T) = R_{e[1,2]} \cdot \left(1 + \mathtt{tc1rc} \cdot dT + \mathtt{tc2rc} \cdot dT^2\right) \tag{30}$$

and again the temperature coefficient in (30) is limited to a lower value of 0.01. The anomalous increase in conductance with Vds for some p-body resistors is due to contact resistance self-heating and negative temperature coefficients; this was pointed out in [3].

The parasitic diode saturation currents vary with temperature as

$$I_{sa}(T) = \mathtt{isa} \cdot rT^{\mathtt{xis/na}} \cdot \exp\left(-\mathtt{ea} \cdot \frac{1 - rT}{\mathtt{na} \cdot \phi_t}\right) \tag{31}$$

$$I_{sp}(T) = \mathtt{isp} \cdot rT^{\mathtt{xis/np}} \cdot \exp\left(-\mathtt{ea} \cdot \frac{1 - rT}{\mathtt{np} \cdot \phi_t}\right) \tag{32}$$

where $\phi_t = kT/q$ is the thermal voltage. The temperature dependence of the junction built-in potentials is

$$P_a(T) = \texttt{pa} \cdot rT - 3 \cdot \phi_t \cdot \ln(rT) - \texttt{ea} \cdot (rT - 1) \tag{33}$$

$$P_p(T) = \texttt{pp} \cdot rT - 3 \cdot \phi_t \cdot \ln(rT) - \texttt{ea} \cdot (rT - 1) \tag{34}$$

with a physically based modification to smoothly limit the potential to zero for high temperatures, and not allow it to become negative. The area and perimeter junction zero-bias capacitance temperature variations are

$$C_{ja} = \texttt{cja} \cdot \left(\frac{\texttt{pa}}{P_a T}\right)^{\texttt{ma}} \tag{35}$$

and

$$C_{jp} = \texttt{cjp} \cdot \left(\frac{\texttt{pp}}{P_p T}\right)^{\texttt{mp}}. \tag{36}$$

The flicker noise coefficient varies with temperature as

$$k_{FN}(T) = \texttt{kfn} \cdot (1 + \texttt{tc1kfn} \cdot dT) \tag{37}$$

where `kfn` and `tc1kfn` are model parameters (and the resulting is clipped to zero as a lower limit).

The breakdown voltage and ideality factor vary with temperature as

$$V_{bv}(T) = \texttt{vbv} \cdot \left(1 + \texttt{tc1vbv} \cdot dT + \texttt{tc2vbv} \cdot dT^2\right), \tag{38}$$

$$n_{bv}(T) = \texttt{nbv} \cdot (1 + \texttt{tc1nbv} \cdot dT). \tag{39}$$

8 Bias Dependence of Resistor Body Current

The r3_cmc model includes three basic forms of bias dependence. First, from the depletion (*p-n* junction or MOS) pinching of the conducting channel of the resistor. Second, from velocity saturation. And third, from self-heating.

The basic *p-n* junction depletion pinching bias dependence comes from the analysis of [4], with the simplification of [5] (which merges the vertical and lateral bias dependence into a single bias dependent form with geometry dependent parameters). Further improvements are taken from [6], including improved modeling of pinch-off and velocity saturation. The applicability of the same general form of bias dependence for poly resistors, where the MOS depletion effect pinches the resistor body, was shown in [7]. The fundamental form of the depletion pinching model is

$$I_{depl} = g \cdot V_{21}, \quad g = gf \cdot \left(1 - df \cdot \sqrt{dp + V_i}\right), \quad V_i = V_{21} + 2 \cdot V_{1c} \tag{40}$$

where $V_{21} = V(\mathtt{i2}) - V(\mathtt{i1})$ and $V_{1c} = V(\mathtt{i1}) - V(\mathtt{nc})$. Here dp is the depletion potential, df is the depletion factor, and gf is the conductance factor; these are determined from instance and model parameters and temperature, as detailed in the previous sections.

The velocity saturation model is from [5], and is implemented as an effective mobility reduction factor $1+r_\mu$ that divides the conductance factor in (40). The model for r_μ is smooth and symmetric, has value 0 when $V_{21} = 0$, and asymptotically approaches $(E - ecorn)/ecrit$ for large field $E = V_{21}/(\mathit{leff_um} + \mathtt{dxlsat})$

$$r_\mu = \sqrt{\left(\frac{E - E_{ce}}{2 \cdot ecrit}\right)^2 + du_e} + \sqrt{\left(\frac{E + E_{ce}}{2 \cdot ecrit}\right)^2 + du_e} - \sqrt{\left(\frac{E_{ce}}{ecrit}\right)^2 + 4 \cdot du_e} \tag{41}$$

(see Fig. 3) where $E_{ce} = \sqrt{ecorn^2 + (2 \cdot \mathtt{du} \cdot ecrit)^2} - 2\,\mathtt{du} \cdot ecrit$ and $du_e = \mathtt{du} \cdot E_{ce}/ecrit$.

The V_{21} used in the above expressions is smoothly limited so as not to exceed a saturation voltage V_{sat}, which is calculated as the V_{21} at which the output conductance becomes zero. To determine V_{sat}, a slightly modified form of the velocity saturation model (41) is used (the asymptotic form noted above), that allows closed form solution and guarantees that any imprecision in calculation of V_{sat} is such that the output conductance at saturation is positive, so that there are no "wiggles" around the transition to saturation. The smooth transition is implemented via [8]

$$V_{21,eff} = \frac{2V_{21} \cdot V_{sat}}{\sqrt{(V_{21} - V_{sat})^2 + 4 \cdot ats_i} + \sqrt{(V_{21} + V_{sat})^2 + 4 \cdot ats_i}} \tag{42}$$

where $ats_i = \mathtt{ats}/(1 + \mathtt{atsl}/\mathit{leff_um})$ controls the limiting. This limiting function differs from those often used in compact MOSFET models; it preserves symmetry. The control voltage used is also limited, to the pinch-off voltage

$$V_{1c,eff} = V_{po} - \mathtt{nst} \cdot \phi_t \cdot \ln\left[1 + \exp\left(\frac{V_{po} - V_{1c}}{\mathtt{nst} \cdot \phi_t}\right)\right], \quad V_{po} = \frac{1}{2 \cdot df^2} - 0.5 \cdot dp, \quad \phi_t = kT/q. \tag{43}$$

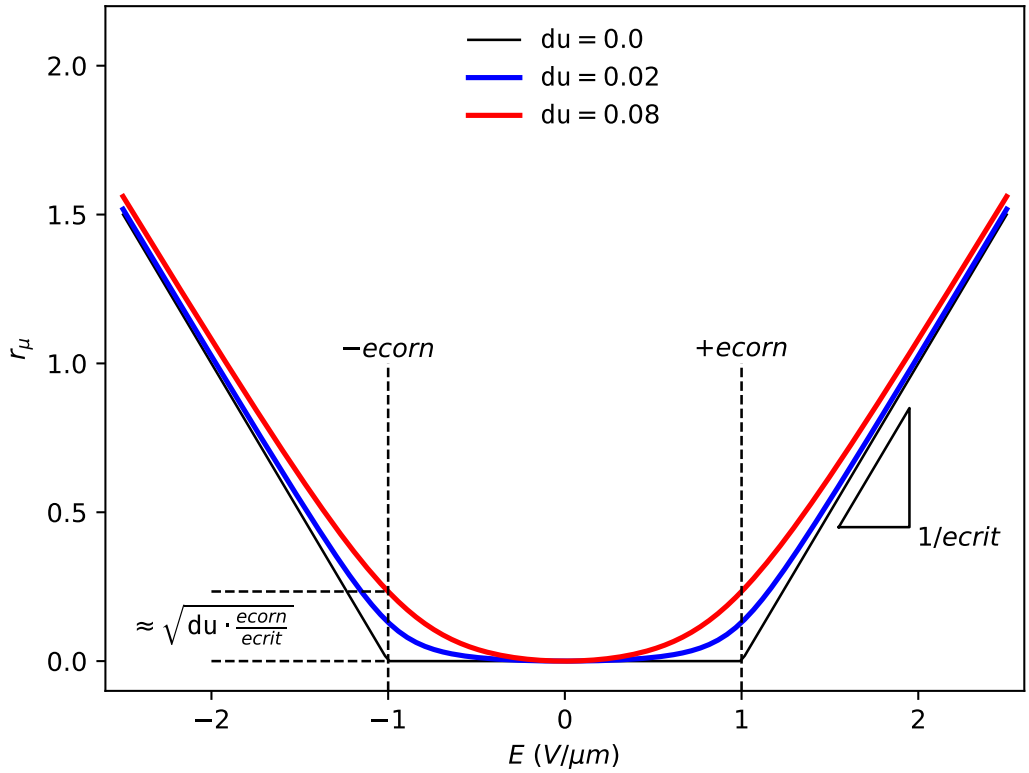

Figure 3: r_μ factor used in the velocity saturation model.

Pinch-off behavior is primarily of importance for JFETs, and four models, selectable via the `sw_accpo` switch, are available. The default is `sw_accpo` $= 0$, which is backwards-compatible with version 1.0.0. The next computationally simplest, and therefore fastest to simulate, limiting is selected with `sw_accpo` $= 1$, however this model only fairly crudely approximates the physically expected $1 - \exp(-V_{21}/\phi_t)$ variation of I_{21} with V_{21} in full pinch-off. Setting `sw_accpo` $= 2$ selects a model that more accurately approximates that behavior, at the expense of increased computation time, and `sw_accpo` $= 3$ selects an even more accurate, but slightly more computationally expensive, form. A minimum conductance is enforced in full pinch-off to avoid numerical computation issues.

The self-heating affects the current through the temperature variation of the model parameters, primarily the sheet resistance. The current flowing between ports `n2` and `n1` in Fig. 1 is then

$$I_{21} = \frac{I_{depl}}{1 + r_\mu}. \tag{44}$$

9 Bias Dependence of Parasitics

If there are no area or perimeter component of saturation current, e.g. for poly resistors,

$$I_{p1} = I_{p2} = 0. \tag{45}$$

If there are area and/or perimeter components of saturation current, e.g. as for diffused resistors, the parasitic diode currents are

$$\begin{aligned} I_{p1} &= p1_um \cdot I_{sp}(T) \cdot \left\{ \exp\left[V_{c1}/(\mathtt{np} \cdot \phi_t)\right] - 1 \right\} \\ &\quad + a1_um2 \cdot I_{sa}(T) \cdot \left\{ \exp\left[V_{c1}/(\mathtt{na} \cdot \phi_t)\right] - 1 \right\} + gmin \cdot V_{c1} \qquad (46) \\ I_{p2} &= p2_um \cdot I_{sp}(T) \cdot \left\{ \exp\left[V_{c2}/(\mathtt{np} \cdot \phi_t)\right] - 1 \right\} \\ &\quad + a2_um2 \cdot I_{sa}(T) \cdot \left\{ \exp\left[V_{c2}/(\mathtt{na} \cdot \phi_t)\right] - 1 \right\} + gmin \cdot V_{c2} \qquad (47) \end{aligned}$$

where $V_{c1} = V(\mathtt{nc}) - V(\mathtt{i1})$, $V_{c2} = V(\mathtt{nc}) - V(\mathtt{i2})$, and $gmin$ is a small conductance added by some simulators to improve convergence. Note that, when $\mathtt{sw_accpo} > 0$, V_{c1} and V_{c2} are limited to pinch-off by a smoothing equation. Each individual component of the diode currents is linearized for forward biases greater than the voltage at which the component is `imax`.

The breakdown currents, which are added to each parasitic current, are

$$I_{b1} = -\mathtt{ibv} \cdot \left(\exp\left\{-\left[V_{c1} + V_{bv}(T)\right] / \left[n_{bv}(T) \cdot \phi_t\right]\right\} - \exp\left\{-V_{bv}(T) / \left[n_{bv} \cdot (T)\, \phi_t\right]\right\} \right), \tag{48}$$

$$I_{b2} = -\mathtt{ibv} \cdot \left(\exp\left\{-\left[V_{c2} + V_{bv}(T)\right] / \left[n_{bv}(T) \cdot \phi_t\right]\right\} - \exp\left\{-V_{bv}(T) / \left[n_{bv} \cdot (T)\, \phi_t\right]\right\} \right), \tag{49}$$

and each of these is linearized for reverse biases greater than the voltage as which the magnitude of the current is `imax`.

The parasitic capacitances comprise a bias independent component (intended for poly resistor modeling) and a bias dependent component (intended for diffused resistor modeling). The capacitances are implemented as bias dependent charges, but the resulting capacitances are given here:

$$\begin{aligned} C_{p1} &= p1_um \cdot \left\{ \mathtt{cp} + \frac{C_{jp}(T)}{[1 - V_{c1}/P_p(T)]^{\mathtt{mp}}} \right\} + a1_um2 \cdot \left\{ \mathtt{ca} + \frac{C_{ja}(T)}{[1 - V_{c1}/P_a(T)]^{\mathtt{ma}}} \right\} \qquad (50) \\ C_{p2} &= p2_um \cdot \left\{ \mathtt{cp} + \frac{C_{jp}(T)}{[1 - V_{c2}/P_p(T)]^{\mathtt{mp}}} \right\} + a2_um2 \cdot \left\{ \mathtt{ca} + \frac{C_{ja}(T)}{[1 - V_{c2}/P_a(T)]^{\mathtt{ma}}} \right\}. \qquad (51) \end{aligned}$$

The forward bias junction capacitance components are modified so that when the junction voltage (V_{c1} or V_{c2}) reaches `fc` multiplied by the associated built-in potential, the capacitance becomes linear in voltage, to avoid the singularity at the built-in potential. If the smoothing parameters `aja` and `ajp` are positive, then the transition from depletion to linear capacitance is done smoothly and not abruptly.

The thermal resistance and capacitance for the self-heating model are linear. The thermal resistance has a temperature dependence through the parameter `tegth`, but the thermal capacitance does not

depend on temperature. The thermal power used for self-heating modeling is the sum of the powers of all dissipative (non-storage) elements in the equivalent circuit; i.e. the resistor body, the two end resistances, and two parasitic current sources.

10 Noise

The noise model comprises two body components, a thermal (white) noise component and a flicker (1/f) noise component, thermal noise components for each contact resistance, and short noise components for each parasitic diode. These components are noise current spectral density (in A^2/Hz) that are implemented as a noise current sources in parallel with the associated element.

The thermal noise component of the resistor body is based on its DC conductance,

$$i^2_{thermal,body} = 4 \cdot k \cdot T_K \cdot G_{eff}(T) \tag{52}$$

where K is Boltzmann's constant, T_K is the device temperature (in Kelvin, including the effect of self-heating), and is the effective conductance of the resistor (at the temperature). Similarly, the thermal noise of each end resistances is

$$i^2_{thermal,end} = 4 \cdot k \cdot T_K / R_e(T). \tag{53}$$

The flicker noise component is DC current dependent [9], and scales with geometry per the physical restrictions in [10],

$$i^2_{flicker,body} = K_{FN}(T) \cdot \left(\frac{I_{21}}{W}\right)^{\texttt{afn}} \cdot \frac{W}{L} \cdot \frac{1}{f^{\texttt{bfn}}} \tag{54}$$

where f is frequency (in Hz), `afn` and `bfn` are model parameters, $K_{FN}(T)$ is the temperature dependent flicker noise coefficient (37), I_{21} is the DC current in the resistor body (44), and W and L are the resistor width and length, respectively, in units of micron (μm). If the switch parameter for flicker noise geometry calculation `sw_fngeo` is 0 ("false") then and are design geometries, *w_um* and *l_um*, respectively, else if it is 1 ("true") then W and L are effective geometries, *weff_um* and *leff_um* respectively.

The shot noise components are

$$i^2_{shot,diode} = 2 \cdot q \cdot I_{diode} \tag{55}$$

for each parasitic diode, where I_{diode} is the current in the diode.

Note that if self-heating is included, then possibly there is a frequency dependence to the flicker noise because of the thermal time constant. There is no data to verify this at present so a frequency independent noise current spectral density is used.

11 Operating Point Information

Name	Units	Description
v	V	voltage across resistor body
ibody	A	current through resistor body
power	W	dissipated power
leff_um	μm	effective electrical length
weff_um	μm	effective electrical width
r0	Ω	zero-bias resistance
r_dc	Ω	DC resistance (including bias dependence)
r_ac	Ω	AC resistance (including bias dependence)
rth	K/W	thermal resistance
cth	sW/K	thermal capacitance
dt_et	K	self-heating temperature rise

12 Statistical Variation

The r3_cmc model includes both global (inter-die, correlated between individual devices) and local (mismatch, uncorrelated between individual devices) variations. These can be added "on top" of a core model using sub-circuits, however this can involve increased complexity in model parameter files and increased computational overhead during simulation. Therefore, statistical variation is "built-in" to the r3_cmc model, including instance parameters for control of mismatch variation for individual devices.

Besides convenience and efficiency, the statistical variation modeling in r3_cmc naturally embodies the geometry dependence of total variation in a device, which is not possible with statistical modeling based on a geometry independent global variation and geometry dependent correlation coefficients. And because it is based on independent statistical parameters for global variation and instance specific local variation, it does not require generation of correlated samples for distributional (i.e. Monte Carlo-like) simulation; if correlations were used then $N(N-1)/2$ of them are required for each statistical parameter for each of devices.

Statistical variations are modeled in three parameters; the sheet resistance, the effective length variation, and the effective width variation. These are considered as the primary physical process parameters that determine the resistor behavior. At present there is no variation (global or local) in other physical quantities such as contact resistance, other parasitics (zero-bias depletion capacitance for diffused resistors varies with doping), or the parameters that control the nonlinearity of the model. If experimental data that show that linkage to more fundamental physical quantities, such as doping levels and layer thicknesses, is required to model correlations and statistical variations, this will be added in the future.

The local variation of the effective width is controlled by line edge roughness in the length dimension; its variance is therefore inversely proportional to the resistor length L. The local variation of the effective length is controlled by line edge roughness in the width dimension; its variance is therefore inversely proportional to the resistor width W. The local variation of the sheet resistance is controlled by random dopant fluctuations; its variance is therefore inversely proportional to the area of the resistor, WL. For flexibility in fitting experimental data, the sw_mmgeo flag allows the controlling geometries W and L to be either drawn or effective (as calculated before the statistical variations are applied, to avoid an implicit dependency that requires an iterative solution).

The total variance of a parameter is the sum of the variances of the global variance (which is independent of geometry) and the local variance (which depends on geometry $\vec{g}$, which can include area, width, and length),

$$\sigma_{total}^2 = \sigma_{global}^2 + \sigma_{local}^2\left(\vec{g}\right). \tag{56}$$

Note that this naturally embodies the geometry dependence of the overall variance of a particular parameter. For statistical simulation, the perturbations of the global variation and the individual instance variation are expected to be statistically independent. But "proper" statistical simulation of a circuit requires inclusion of both global parameters and local parameters for every instance of a device type in a circuit. This can cause the number of statistical parameters included in a statistical simulation to increase proportionally with the number of devices in the circuit, with a concomitant explosion in the number of (local) statistical parameters needed to be included for a

"proper" analysis. This is, for brute force statistical simulation, clearly impractical.

The r3_cmc model therefore includes a mechanism for more efficiently accounting for the geometry dependence of the overall variation. The sw_mman switch is provided to allow specification on an instance-by-instance basis of whether a device is being included in mismatch analysis. If yes, then both global and local (instance specific) statistical variation parameters are expected to be generated for each device instance, and the global and local variations are modeled separately. If no, which is appropriate for devices for which local variation is not expected to affect circuit performance, then the global variance for a device is adjusted to be the total variance for that device. This appropriately models the geometry dependent total variance for the device, with the consequence that it makes the total variation completely correlated between all devices (that are not selected for individual mismatch analysis); this will cause overestimation of the variation of the circuit performances, i.e. the simulations from this will be pessimistic.

If mismatch analysis is selected, then the statistical variations are

$$\mathit{weff_um} = \mathit{weff_um}_{nom} + \texttt{nsig_w} \cdot \texttt{sig_w} + \frac{\texttt{nsmm_w} \cdot \texttt{smm_w}}{\sqrt{m \cdot L}} \tag{57}$$

$$\mathit{leff_um} = \mathit{leff_um}_{nom} + \texttt{nsig_l} \cdot \texttt{sig_l} + \frac{\texttt{nsmm_l} \cdot \texttt{smm_l}}{\sqrt{m \cdot W}} \tag{58}$$

$$\mathit{rsh} = \mathit{rsh}_{nom} \cdot \exp\left[0.01 \cdot \left(\texttt{nsig_rsh} \cdot \texttt{sig_rsh} + \frac{\texttt{nsmm_rsh} \cdot \texttt{smm_rsh}}{\sqrt{m \cdot WL}}\right)\right] \tag{59}$$

where the nominal values are those defined in the section on geometry dependence and m is the multiplicity factor of the instance. (The above expressions are used to update the effective geometries and resistance values, and all previous model equations actually use the values calculated in (57) through (59), however for clarity of presentation and ease of interpretation the previous equations are not cluttered with the statistical variations).

Note that the variations in effective length and width are absolute, and are additive, and that the variation in sheet resistance is multiplicative. For small variations $\exp(x) \approx (1+x)$, hence the rsh variation is relative (it is more natural to think in terms of a % variation than an absolute variation). For large variations, as can be seen in some resistors, statistical sampling can generate very small or negative values of rsh, which are unphysical. Quantities with large variations typically exhibit a log-normal distribution, and the exponential mapping in (59) transforms the normally distributed basic statistical parameters into a log-normal distribution for rsh if the variation is large. Note that strictly the unit "%" for the standard deviations of rsh is only for a small variation; if the variation is large then the exponential transformation in (59) modifies this.

This approach allows statistical modeling via uncorrelated normal variables, yet can capture log-normal distributions and correlations between parameters, via the dependencies on the fundamental process parameters that control the device behavior. Note that mismatch is modeled via independent perturbations in individual devices, which is physically correct. To simulate mismatch between two devices the mismatch instance parameters for both devices must be selected for statistical perturbation, and this easily extends to more than two devices, and implicitly accounts for geometry differences between different devices. If mismatch is characterized from differential measurements between two identically sized devices, then the measured standard deviations need to be divided by $\sqrt{2}$ when mapped into the model parameters smm_w, smm_l, and smm_rsh. If

mismatch analysis is not selected, then the total variance in (56) is used as the global variance,

$$\mathit{weff_um} = \mathit{weff_um}_{nom} + \texttt{nsig_w} \cdot \sqrt{\texttt{sig_w}^2 + \texttt{smm_w}^2/(m \cdot L)} \tag{60}$$

$$\mathit{leff_um} = \mathit{leff_um}_{nom} + \texttt{nsig_l} \cdot \sqrt{\texttt{sig_l}^2 + \texttt{smm_l}^2/(m \cdot W)} \tag{61}$$

$$\mathit{rsh} = \mathit{rsh}_{nom} \cdot \exp\left\{0.01 \cdot \texttt{nsig_rsh} \cdot \left[\texttt{sig_rsh}^2 + \texttt{smm_rsh}^2/(m \cdot W \cdot L)\right]\right\}. \tag{62}$$

Note that the nsig parameters should be equated to global statistical variables in model files, as they are model parameters, not instance parameters. These parameters then should vary with case/corner and distributional simulations.

13 Notes on Parameter Extraction

This section provides some information that can help in setting up parameter extraction algorithms. After fairly extensive development and testing of difference possible approaches, the techniques detailed in [11] have proven to be robust, and are summarized here. The overall process can be broken down into the following steps:

- calculate the zero-bias conductance $G_z(V_{1c}) = 1/R_z(V_{1c})$ for each geometry, temperature, and control port bias V_{1c}, for $V_{21} = 0$
- from $G_z(0)$ calculate basic resistance and temperature coefficients and their geometry dependence
- calculate the depletion pinching parameters df and dp for each device from $G_z(V_{1c})$
- extract velocity saturation and thermal conductance parameters
- perform an overall global optimization

Note that the techniques for the first and third items are different for poly and diffused resistors. Although the data are $I_{21}(V_{21}, V_{1c})$ extraction should always be done based on $G = I_{21}/V_{21}$.

The procedures outlined here are for the core resistor DC current, characterization of parasitic resistances, junction currents, and capacitances are not covered. It is fairly straightforward to determine them using standard techniques.

G_z Calculation

It is not possible to directly calculate G_z because it is the value of I_{21}/V_{21} at $V_{21} = 0$. It can be difficult to determine G_z as $\lim_{V_{21}\to 0} I_{21}/V_{21}$ because G becomes "noisy" for small values of V_{21}. A robust way to determine G_z is to fit an appropriate function to $G(V_{21}, V_{1c})$ for each V_{1c} individually and use that function to calculate $G_z(V_{1c})$. The procedure is different for diffused and poly resistors, but for both, data around $V_{21} = 0$ that are too "noisy" need to be filtered out.

For diffused resistors, serendipitously the effect of self-heating at low and moderate E is essentially the same as the effect of velocity saturation. So, simply fit the function

$$G(V_{21}, V_{1c}) = \frac{G_z(V_{1c}) \cdot \left(1 - df \cdot \sqrt{dp + V_{21} + 2 \cdot V_{1c}}\right)}{(1 + r_\mu) \cdot \left(1 - df \cdot \sqrt{dp + V_{1c}}\right)} \tag{63}$$

(r_μ is given by (41)) to the data, limited to where G is greater than 80% of its maximum value, to avoid data that are more dependent on velocity saturation and/or self-heating than on depletion pinching. Fig. 4 shows fits of (63) to data from a diffused resistor that is significantly affected by all of depletion pinching, velocity saturation, and self-heating. The "noise" at low V_{21} is apparent, as is the accuracy of the extrapolation. This approach is substantially more robust and accurate than fitting a simple polynomial model.

For poly resistors, $G(V_{21})$ is usually noisier than for diffused resistors because poly resistors are significantly more linear than diffused resistors. However, because there are no pn-junctions to

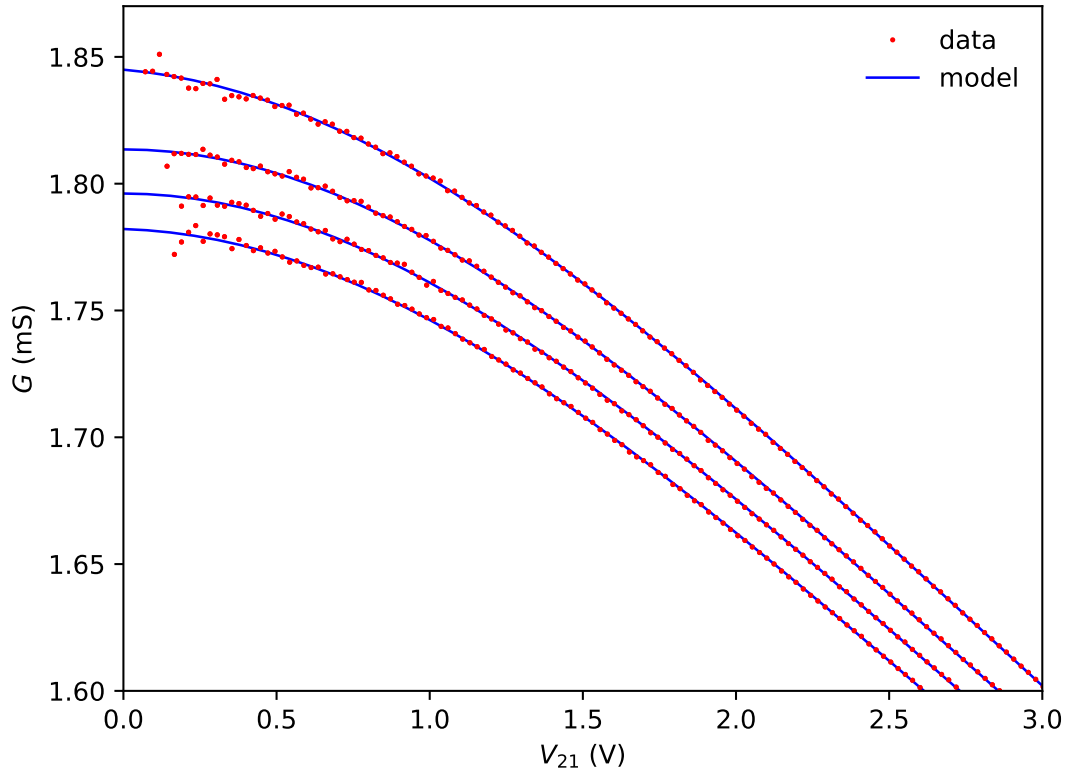

Figure 4: G_z extrapolation for a diffused resistor. $|V_{1c}|$ increases from top to bottom.

forward bias, V_{21} can be swept from negative to positive values, so interpolation, rather than extrapolation, can be used to determine G_z. The depletion pinching effect in poly resistors is so small it can be closely approximated as linear, and self-heating gives a quadratic dependence of G on field at low and moderate fields. In some poly resistors self-heating can be so pronounced that the effect of T_{C2}^{eff} becomes noticeable, which adds a fourth order dependence. Therefore, the function

$$G(V_{21}, V_{1c}) = b_0 + V_{21} \cdot [b_1 + V_{21} \cdot (b_2 + V_{21}^2 \cdot b_4)] \tag{64}$$

should be used for poly resistors. If the contribution of the fourth order term is significant, reduce the range of $\pm V_{21}$ over which the model is fitted; the goal is to accurately model the linear and quadratic components about $V_{21} = 0$. Fig. 5 shows fits of (64) to data from a poly resistor that is significantly affected by self-heating. The "noise" in the data, and the effectiveness of fitting the model (64) to average out the noise and allow accurate interpolation of G_z, are apparent.

Basic Geometry and Temperature Dependence Calculation

The basic geometry dependence of R_z (typically taken to be at $V_{1c} = 0$) is

$$R_z = \texttt{rsh} \cdot \frac{l_um + \texttt{xl} + \texttt{xlw}/w_um}{w_um + \texttt{xw} + \texttt{nwxw}/w_um} \tag{65}$$

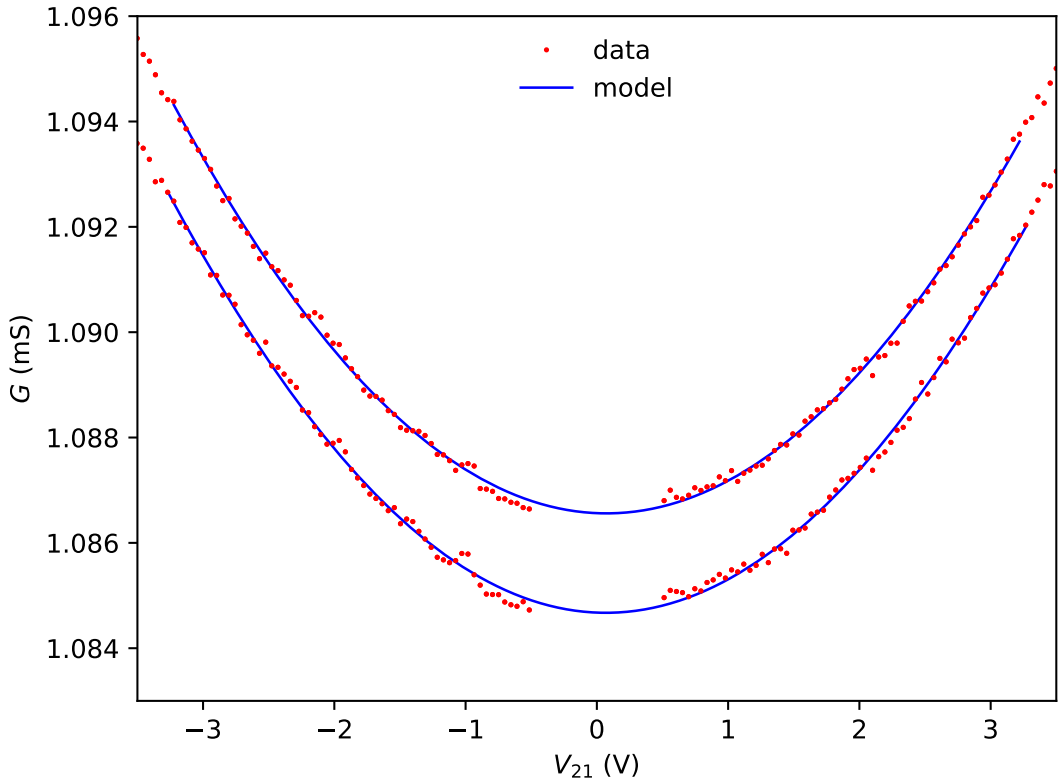

Figure 5: G_z extrapolation for a poly resistor. The magnitude of V_{1c} increases from top to bottom.

which after some simple manipulations gives

$$\begin{aligned}\mathtt{rsh} - \left(\frac{R_z}{l_um}\right)\cdot \mathtt{xw} - \left(\frac{R_z}{l_um \cdot w_um}\right)\cdot \mathtt{nwxw} + \left(\frac{1}{l_um}\right)\cdot(\mathtt{rsh}\cdot\mathtt{xl}) \\ + \left(\frac{1}{l_um \cdot w_um}\right)\cdot(\mathtt{rsh}\cdot\mathtt{xlw}) = \left(\frac{R_z \cdot w_um}{l_um}\right).\end{aligned} \tag{66}$$

R_z, l_um, and w_um are known, so this is a linear equation in five unknowns, `rsh`, `xw`, `nwxw`, $\mathtt{rsh}\cdot\mathtt{xl}$, and $\mathtt{rsh}\cdot\mathtt{xlw}$. From five or more appropriate geometry devices, (66) can be solved to give the basic parameters `rsh`, `xw`, `nwxw`, `xl`, and `xlw` that model the zero-bias resistance and its geometry dependence.

From $R_z(T)$ the first and second order temperature coefficients can be calculated for each geometry. From four or more appropriate geometries, (10) and (11) can then be solved for the temperature coefficient geometry dependence parameters.

Depletion Pinching Parameter Calculation

The depletion pinching modulation of the channel conductance depends on both V_{21} and V_{1c}. Velocity saturation and self-heating have no effect at $V_{21} = 0$, but for short resistors their effect is noticeable even for low V_{21}, see Figs. 4 and 5. In addition, because V_{1c} affects depletion pinching

at both ends of the channel but V_{21} affects only one end, V_{1c} has twice as much depletion pinching influence as V_{21}. Depletion pinching parameters should therefore be determined from $G_z(V_{1c})$.

For diffused resistors, (40) at $V_{21} = 0$ can be manipulated to give

$$-2 \cdot V_{1c} = \left(\frac{1}{d_f^2} - d_p \right) - \frac{2}{d_f^2 \cdot g_f} \cdot G_z(V_{1c}) + \frac{1}{d_f^2 \cdot g_f^2} \cdot G_z(V_{1c})^2 \,. \tag{67}$$

A linear regression of G_z and G_z^2 on V_{1c} for three or more values of V_{1c} allows d_f and d_p to be calculated for each device geometry and temperature. Details, and an alternative approach that can be used if data for only two V_{1c} values are available or if it is not possible to extrapolate G_z reliably, are available in [11].

Poly resistors are highly linear, so $G_z(V_{1c})$ provides only one piece of information, the linearity coefficient [11]

$$l_1 = \left(\frac{1}{G} \frac{\partial G}{\partial V_{1c}} \cdot \right)_{V_{21}=V_{1c}=0} = \frac{d_f}{\sqrt{d_p}} \cdot \frac{1}{1 - d_f \cdot \sqrt{d_p}} \,. \tag{68}$$

Now, d_p for a poly resistor is essentially [12] $\gamma^2/2$ where γ is the body effect coefficient of the resistor treated as an upside-down MOS transistor. Because poly resistors sit on thick oxides, to minimize parasitic capacitance and maximize linearity, d_p can be large, often many hundreds of Volts. To fit the measured l_1 this requries d_f to be large as well, but this can, and does, cause numerical problems with the $1 - d_f\sqrt{d_p}$ term. With l_1 of (68) determined from the interpolated $G_z(V_{1c})$, d_p can be calculated from [11]

$$d_p = \frac{\epsilon_s}{l_1 \cdot t_b \cdot C'_{ox}} \tag{69}$$

where ϵ_s is the permittivity of silicon, t_b is thickness of the polysilicon body of the resistor and C'_{ox} is the capacitance per unit area of the oxide under the resistor. d_f then follows as

$$d_f = \frac{1}{\sqrt{d_p} \cdot [1 + 1/(l_1 \cdot d_p)]} \,. \tag{70}$$

For both diffused and poly resistors, fitting (8), (7), and (27) to the values of d_f and d_p determined for each device geometry and temperature gives the geometry and temperature parameters for d_f and d_p.

Velocity Saturation and Self-Heating Parameter Calculation

Poly resistors are not affected by velocity saturation, so set `ecrit` $= 0$ and `ecorn` $= 0$ to turn velocity saturation modeling off. For diffused resistors, for n-body devices initialize `ecrit` $= 4$, `ecorn` $= 0.4$, and `du` $= 0.02$ (these are their default values), for p-body devices initialize `ecrit` $= 1.2$, `ecorn` $= 0.12$, and `du` $= 0.02$. For diffused resistors of both body polarity types, set `sw_vsatt` $= 1$; this turns on substantially improved modeling of velocity saturation over temperature, physically linked to resistance, i.e. mobility, variation with temperature (for backward compatibility the default is to turn this off). For both diffused and poly resistors, initialize `gthc` $= 10^{-5}$.

The most effective way to get initial estimates of self-heating parameters is from the r_μ factor. For both velocity saturation and self-heating, basic symmetry dictates that they are quadratic in field at low field. From (40) and (44),

$$r_\mu = r_\mu^{vs} + r_\mu^{sh} = \frac{1}{G(V_{21}, V_{1c}) \cdot R_z(V_{1c})} \frac{1 - d_f \sqrt{d_p + V_{21} + 2 \cdot V_{1c}}}{1 - d_f \cdot \sqrt{d_p}} - 1 \tag{71}$$

where the added superscripts vs and sh are for the velocity saturation and self-heating components, respectively. It can be shown that

$$\frac{\partial r_\mu}{\partial V_{21}^2} \approx \frac{2 \cdot \mathtt{du}}{E_{ce}^2 \cdot (1 + 4 \cdot \mathtt{du} \cdot ecrit/E_{ce})^{3/2}} \cdot \frac{1}{\mathit{leff_um}^2} + \frac{T_{C1}^{eff}}{g_{TH} \cdot R_z} \tag{72}$$

where the first component is from velocity saturation and the second is from self-heating. r_μ can be determined from (71), all quantities on the right hand side are known (directly or from previous extraction steps). This removes the effect of depletion pinching from the data. From that, the slope $\partial r_\mu / \partial V_{21}^2$ can be determined, for diffused resistors the velocity saturation component can be subtracted (it is zero for poly resistors), and g_{TH} can be calculated. This should be done based on long resistors, because that mazimizes the influence of self-heating compared to velocity saturation. From g_{TH} as a function of width the area and perimeter components of thermal conductance can be calculated.

Final Optimization

The basic goal is to model the deviation from linearity (which is important for distortion modeling), so a final "polishing" of the intitial parameters extracted as outlined above should target that quantity [13]. Because of local variation (mismatch) it can be difficult to merge data from different devices for model parameter extraction. Measuring multiple sites and taking the median of the data can help, particularly to determine the basic resistance and temperature parameters. But for highly linear resistors, e.g. poly resistors, the difference between measurements and the model can be dominated by local variation or inaccuracy in fitting R_z (which is already optimized as solution of (66) gives a least-squares fit). Therefore, and this is extremely important, a final optimization of the "shape" parameters of R3, the depletion pinching, self-heating, and (for diffused resistors) velocity saturation, parameters, should scale the modeled conductance by the ratio R_z^{model}/R_z^{meas}. This removes any offset in modeling R_z so only optimizes fitting of the nonlinearity.

c_{TH} can only be determined from the frequency dependence of the small-signal resistance, and this is not commonly available as it requires s-parameter test structures and measurements. Data from a wide variety of devices indicate that thermal time constants for integrated devices vary from about 0.1 to 10.0 μs. with 1 μs being a typical value. If no s-parameter data are available, set $c_{TH} = 10^{-6} \cdot g_{TH}$.

14 References

References

[1] *Verilog-AMS Language Reference Manual*. Available for download from Accellera Organization, Inc. at `https://accellera.org/downloads/standards/v-ams`

[2] C. C. McAndrew, S. Sekine, A. Cassagnes, and Z. Wu, "Physically Based Effective Width Modeling of MOSFETs and Diffused Resistors," *Proc. IEEE ICMTS*, pp. 169-174, 2000.

[3] K. Banerjee, A. Ameraskera, G. Dixit, and C. Hu, "Temperature and Current Effects on Small-Geometry-Contact Resistance," *Proc. IEEE IEDM*, pp. 115-118, 1997.

[4] R. V. H. Booth and C. C. McAndrew, "A 3-Terminal Model for Diffused and Ion-Implanted Resistors," *IEEE Trans. Electron Dev.*, vol. 44, no. 5, pp. 809-814, May 1997.

[5] C. C. McAndrew, "R3, an Accurate JFET and 3-Terminal Diffused Resistor Model," *Proc. Nanotech WCM*, vol. 2, pp. 86-89, 2004.

[6] C. McAndrew, "R3 (Version 2.0.0)." nanoHUB. doi:10.4231/D3QB9V64G, available at `https://nanohub.org/publications/26/1` (2014).

[7] J. Victory, C. C. McAndrew, J. Hall, and M. Zunino, "A 4-Terminal Compact Model for High Voltage Diffused Resistors with Field Plates," *IEEE J. Solid-State Circuits*, vol. 33, no. 9, pp. 1453-1458, Sep. 1998.

[8] C. C. McAndrew, "Useful Numerical Techniques for Compact Modeling," *Proc. IEEE ICMTS*, pp. 121-126, 2002.

[9] R. Brederlow, W. Weber, C. Dahl, D. Schmitt-Landsiedel, and R. Thewes, "A physically based model for low-frequency noise of poly-silicon resistors," *Tech. Digest IEDM*, pp. 89-92, 1998.

[10] C. C. McAndrew, G. Coram, A. Blaum, and O. Pilloud, "Correlated noise modeling and simulation," *Proc. NanoTech WCM*, pp. 40-45, 2005.

[11] C. C. McAndrew and T. Bettinger, "Robust parameter extraction for the R3 nonlinear resistor model for diffused and poly resistors," *IEEE Trans. Semicond. Manuf.*, vol. 26, no. 4, pp. 555-563, Nov. 2012.

[12] K. Xia, C. C. McAndrew, and B. Grote, "Dual-gate JFET modeling I: generalization to include MOS gates and efficient method to calculate drain-source saturation voltage," *IEEE Trans. Electron Devices*, vol. 63, no. 4, pp. 1408-1415, Apr. 2016.

[13] P. Humphries, CMC Meeting, Dec. 2006.